Physica C: Superconductivity and its applications 546 (2018) 6–10

Contents lists available at ScienceDirect

Physica C: Superconductivity and its applications

journal homepage: www.elsevier.com/locate/physc

Type-I superconductivity in carbon-coated Sn nano-spheres

L. Shani[a], V.B. Kumar[b], A. Gedanken[b], I. Shapiro[a], B.Ya. Shapiro[a], A. Shaulov[a], Y. Yeshurun[a,*]

[a] Department of Physics and Institute of Nanotechnology and Advanced Materials, Bar-Ilan University, 52900 Ramat-Gan, Israel
[b] Department of Chemistry and Institute of Nanotechnology and Advanced Materials, Bar-Ilan University, 52900 Ramat-Gan, Israel

ARTICLE INFO

Article history:
Received 13 June 2017
Revised 5 November 2017
Accepted 6 December 2017
Available online 7 December 2017

ABSTRACT

Tin spheres of diameter ~120 nm and ~1400 nm coated with sub-nanometer carbon layers were fabricated, using a sonochemical technique. Samples of both spheres reveal a type-I superconducting behavior characterized by super-critical fields and an intermediate state manifested by a gradual increase of the magnetization to zero. However, the small and large tin spheres exhibit a similar critical field, H_c, contrary to the expected increase in H_c in spheres with size smaller than the coherence length (~230 nm). Analysis of the data shows that a relative high degree of carbon doping in the small tin spheres, eliminates the expected size-effect on H_c. Simulations, based on the time dependent Ginzburg-Landau equations, imply that the intermediate state in both measured samples consists of only one superconducting domain surrounded by a normal domain, whereas a rich multi-domain structure is predicted for larger Sn spheres.

1. Introduction

The interest in type-I superconductors has recently revived, investigating samples of size smaller than the superconducting coherence length, ξ, or the penetration depth, λ [1–6]. In such samples, significant deviations from bulk superconducting properties have been predicted and observed. Specifically, a significant enhancement of the critical field, H_c, was observed in nano-size type-I superconductors [4,7–14]. A pitfall in such a study may arise from agglomeration and/or oxidation of the nano-particles. These may be prevented by protecting the particles with various materials. For example, carbon coating is commonly used to protect tin nano-particles [13,15,16].

In this paper we show that the coating process may cause doping of the superconducting material and thus may affect drastically its superconducting properties. We report on magnetization measurements in carbon-coated tin nano-spheres fabricated by a sonochemical technique [15]. The magnetic behavior of two samples were compared: Spheres of diameter ~120 nm (which is in between $\lambda_0 = 34$ nm and $\xi_0 = 230$ nm of bulk tin), and larger spheres of diameter ~1400 nm, both coated with sub-nanometer layers of carbon. Our magnetization measurements show clearly a type-I superconducting behavior of both samples with well-defined 'superheating' and 'supercooling' fields, and an intermediate state manifested by a gradual increase of the magnetization to zero as the superheating field is approached. However, unexpectedly, no significant change was found in the critical field of the small spheres as compared to the large ones. We attribute this result to the doping of the tin spheres with carbon atoms during the coating process. The doping reduces the effective coherence length to below the sphere size, thus eliminating the size effect. To get insight into the intermediate state in tin spheres we performed simulations based on the time dependent Ginzburg-Landau (GL) equations. The simulations show that the structure of the intermediate state depends on the sphere size which, in turn, affect the shape of the magnetization curve.

2. Experimental

Granules of 99.998% pure β tin (Sn) metals were melted and over-layered by silicone oil in a quartz test tube that was gently heated up. The mixture was irradiated for 5 min with 20 kHz ultrasonic energy, forming a grey suspension of particles in the Si-oil. After precipitation, the particles were separated using a centrifuge, washed several times with n-hexane and dried in vacuum, and then two sizes, 'small' and 'large', of Sn spheres were chosen for the magnetic measurements described in the next section. In the following, we refer to the samples with the small and large spheres as 'sample S' and 'sample L', respectively. The size distribution of the two samples, measured by Dynamic Light Scattering (DLS) technique show a distribution maximum for spheres with di-

* Corresponding author.
E-mail address: yeshurun@mail.biu.ac.il (Y. Yeshurun).

https://doi.org/10.1016/j.physc.2017.12.003
0921-4534/

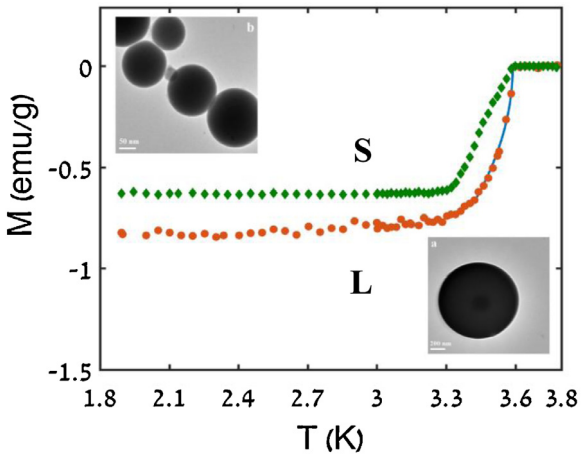

Fig. 1. Magnetization versus temperature measured in the small (S) and large (L) tin spheres. The solid line is a fit to $M \propto (1 - T/T_c)^{1/2}$, see text. The upper and lower insets show TEM images of the small and large spheres, respectively. The scale bars in the images are 50 and 200 nm, respectively.

ameter ~120 nm and ~1400 nm and a full width at half maximum of ~20 nm and ~200 nm for samples S and L, respectively.

Energy-dispersive X-ray spectroscopy (EDS) shows the existence of only one element – Sn – confirming the purity of the sample. X-ray diffraction (XRD) of the small and large particles show multiple peaks, all matching with the database of β tin. No peaks of any other elements were observed, suggesting the presence of a pure metallic tin. CHNSO analysis and Rutherford Backscattering Spectroscopy (RBS) indicates that the amount of carbon atoms varies between 0.27 to 0.41 weights percent in different samples. Transmission Electron Microscope (TEM) images show that the large and small Sn particles are spherical, see insets to Fig. 1. The magnetic measurements described in the next sections were performed using a Superconducting Quantum Interference Device (SQUID - Quantum Design MPMS-5XL) magnetometer.

3. Results

Fig. 1 shows the temperature dependence of the magnetization, measured in samples S (diamonds) and L (circles) with an external field of 30 Oe. The magnetization in sample L approaches zero with a diverging slope, indicating a well-defined transition temperature $T_c = 3.6$ K, consistent with the zero-field transition temperature for bulk tin reported in the literature [4]. Sample S exhibits a gradual approach of *M(T)* to zero with an inflection point around 3.4 K, suggesting a distribution of transition temperatures in this sample.

Magnetization curves were measured at several temperatures between 1.9 and 3.5 K. Typical data at T = 1.9 K are shown in Fig. 2. Both samples exhibit characteristics of type-I superconductors, namely magnetic hysteresis with superheating and supercooling fields [17]. The supercooling fields, H^L_{sc} for sample L, and H^S_{sc} for sample S, are well defined. The superheating field, H^L_{sh}, in the large sample is also well-defined, however, sample S exhibits a long magnetization 'tail', suggesting a distribution of superheating fields. For this sample we define H^S_{sh} for the majority of the spheres by a linear extrapolation of the magnetization at the maximum slope (see the dotted line in the Figure). The measured temperature dependencies of the characteristic fields, H^L_{sh}, H^S_{sh}, H^L_{sc}, and H^S_{sc}, are plotted in Fig. 3. As expected, all these fields decrease to zero as T_c is approached. Notably, at all temperatures the supercritical fields for sample S are bounded by those of sample L, i.e. $H^L_{sh} > H^S_{sh}$ and $H^L_{sc} < H^S_{sc}$.

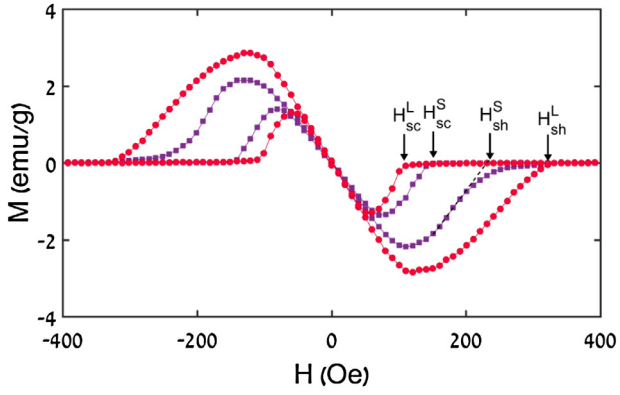

Fig. 2. Magnetization curves at T = 1.9 K for samples S (squares) and L (circles). The characteristic fields, H^L_{sh}, H^S_{sh}, H^L_{sc}, and H^S_{sc}, are indicated by arrows. The dotted line is a linear extrapolation of the magnetization at the maximum slope.

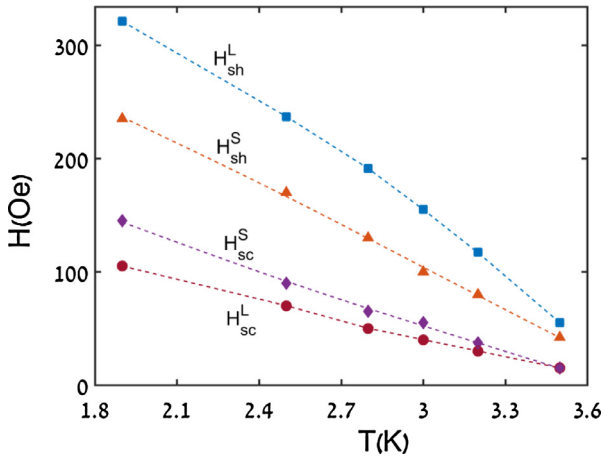

Fig. 3. The measured temperature dependencies of the characteristic fields, H^L_{sh}, H^S_{sh}, H^L_{sc}, and H^S_{sc}. The lines connecting the data points are guide for the eye.

4. Discussion

As mentioned above, the *M(T)* data of Fig. 1 indicate a well-defined transition temperature, T_c, for sample L. Indeed, the *M(T)* data of sample L can be well fitted to $M \propto (1 - T/T_c)^{1/2}$ [17] with $T_c = 3.6$ K, as shown by the solid curve in Fig. 1. The data of sample S, however, cannot be fitted to the above expression, suggesting a distribution of transition temperatures. The origin of this distribution cannot be associated with size distribution of the spheres, since the particle size does not affect T_c (see, e.g., [4]). On the other hand, it is well known that T_c may be affected by doping (see, e.g., [18]). It is thus plausible to attribute the distribution of T_c in sample S to a distribution in the degree of carbon doping in the tin spheres. We note that although sample L went through the same carbon coating process, the carbon doping in this sample is less effective as the ratio of the surface area to the volume of the spheres in this sample is much smaller.

The effect of carbon doping is also manifested in the *M(H)* data of Figs. 2 and 3. These data show that at all temperatures $H^S_{sh} < H^L_{sh}$ and $H^S_{sc} > H^L_{sc}$. The first observation ($H^S_{sh} < H^L_{sh}$) is puzzling as it seems to contradict previous observations in type-I superconductors, demonstrating clearly an increase in H_{sh} as the particle size is reduced [7–12,14,16]. The solution to this puzzle lies in the large increase in the Ginzburg–Landau parameter, $\kappa = \lambda/\xi$, in the small sample, caused by the carbon doping. The increase of κ in the small spheres results from a concurrent decrease in ξ and increase in λ because of carbon doping, as follows from the equa-

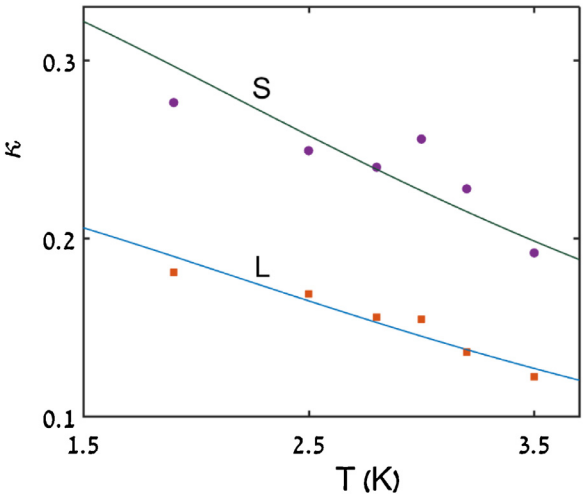

Fig. 4. Temperature dependence of the GL parameter κ as deduced from the measured H_{sh}/H_{sc} for samples S (circles) and L (squares).

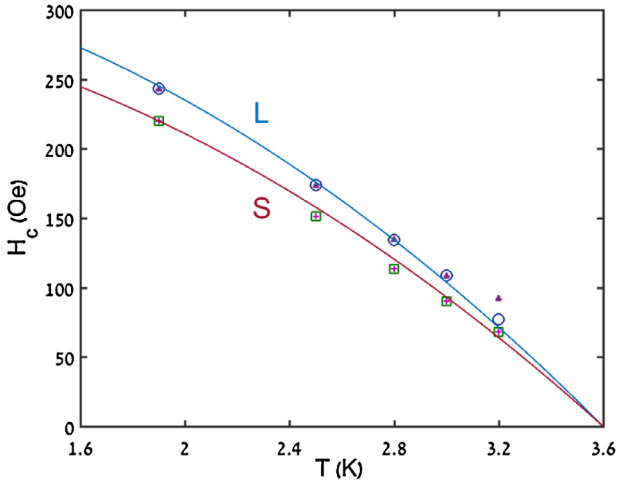

Fig. 5. Calculated temperature dependence of the critical field, H_c, for samples L and S, as deduced from H^L_{sh} (open circles), H^L_{sc} (triangles), H^S_{sh} (open squares) and H^S_{sc} (crosses). The solid lines through the data points describe the empirical approximation $H_c = H_c(0)(1-t^2)$ with (340 Oe, 3.6 K) and (305 Oe, 3.6 K).

tions for ξ and λ in the dirty limit [17]:

$$\xi(T) = 0.85(\xi_0 l)^{1/2}(1-t)^{-1/2}, \tag{1}$$

$$\lambda(T) = 0.62\lambda_L(\xi_0/l)^{\frac{1}{2}}(1-t)^{-1/2}, \tag{2}$$

Where $t = T/T_c$ and l is the mean free path of the electrons. Evidently, the ratio $\kappa = \lambda/\xi$ is inversely proportional to l, thus as l decreases because of doping, κ increases.

The value of κ in both samples can be derived from the measured values of the super-critical fields. For spherical particles [19]:

$$H_{sh} = \frac{2}{3}2^{-1/4}\kappa^{-1/2}H_c \tag{3}$$

$$H_{sc} = 1.69\sqrt{2}\kappa H_c. \tag{4}$$

Thus, the value of κ can be deduced from the ratio

$$H_{sh}/H_{sc} = 0.235/\kappa^{3/2}. \tag{5}$$

The calculated values of κ are shown in Fig. 4 as a function of temperature for both samples. The solid curves through the data points in the Figure are calculated based on the empirical approximation [17]:

$$\kappa = \kappa(0)/\left(1+t^2\right). \tag{6}$$

The fit yields $\kappa(0)$= 0.37 and 0.24 for samples S and L, respectively. Evidently, the values of $\kappa(0)$ for the large spheres are similar to that reported in the literature for bulk tin [3]. However, the deduced values of κ for sample S are significantly larger.

The differences in the values of H_{sh} and H_{sc} between the samples (Figs. 2 and 3) can be explained as resulting from the large difference between the values of κ in these samples. The increase in the value of κ in sample S causes a decrease in H_{sh} (Eq. (3)) and an increase in H_{sc} (Eq. (4)) as compared to the corresponding values in sample L.

Knowledge of the values of κ allows calculation of the critical field, H_c, from either H_{sh} or H_{sc}, using Eqs. (3) or (4), respectively. In Fig. 5 we show H_c *vs.* temperature for sample L as deduced from H^L_{sh} (open circles) and H^L_{sc} (triangles), and for sample S as deduced from H^S_{sh} (open squares) and H^S_{sc} (crosses). The supercooling and superheating fields yield the same H_c values for a given sample; these values are quite similar and close to that reported for clean bulk tin (~300 Oe) [4], implying no effect of the size on H_c. In the following we argue that the size effect expected in sample S is eliminated by a significant reduction of the coherence length to a value smaller than the size of the sample.

The effective coherence length, ξ_{eff}, is related to the coherence length at zero temperature, ξ_0, and the electron mean free path, l, [20]

$$\xi_{\text{eff}} = \xi_0 l/(\xi_0 + l). \tag{7}$$

The value of l can be found from the value of κ at T_c using the dirty limit formula [17]

$$\kappa(T_c) = \frac{0.72\lambda_L(0)}{l}. \tag{8}$$

Inserting $\lambda_L(0) = 34\,nm$ and the experimental value of $\kappa(T_c) = 0.19$ for sample S (Fig. 4), yields $l = 129$ nm. With $\xi_0 \approx 230$ nm, Eq. (7) yields $\xi_{\text{eff}} = 83$ nm. As the doping reduces the value of ξ_{eff} below the size of the sample (~120 nm), no size-effect is expected.

Finally, we note that the shape of the magnetization curves of Fig. 2 are different from that reported in the literature for large, mm-size spheres [21]. Specifically, an approximate linear increase of the magnetization to zero was reported for large Pb sphere whereas Fig. 2 exhibits a much more gradual increase. We attribute this difference to different intermediate structures. To gain insight into the intermediate state in our samples we exploited the time-dependent Ginzburg–Landau (TDGL) scheme [22–26] to numerically calculate the local order parameter and induction in spheres of different radius $R > \xi_{\text{eff}}$, and GL parameter, κ. We start with the dimensionless GL Hamiltonian [26]

$$G\{A,\psi\} = \iiint d^3r\Bigg\{-(1-T)|\psi|^2 + \frac{1}{2}|\psi|^4 + \left|\left(\frac{\partial}{\partial r_i} - iA_i\right)\psi\right|^2\Bigg\}\tau(r) + \kappa^2(\partial\times A - H)^2; \tag{9}$$

where ψ is the order parameter, A the vector potential in units of $\sqrt{2}\ \lambda H_c$, H the applied magnetic field in units of $\sqrt{2}\ H_c$, r the length coordinate scaled by the effective coherence length, τ(r) is a step function incorporating the boundary condition at the sphere surface [27]: $\tau(r) = 1$ for $r < R$ and zero at $r > R$. We solve numerically the time-dependent GL equations in a gauge with zero scalar potential [22–27]

$$\frac{\partial\psi}{\partial t} = -\frac{\delta G}{\delta\psi^*};\quad \frac{\partial A_v}{\partial t} = -\frac{1}{2}\frac{\delta G}{\delta A_v}, \tag{10}$$

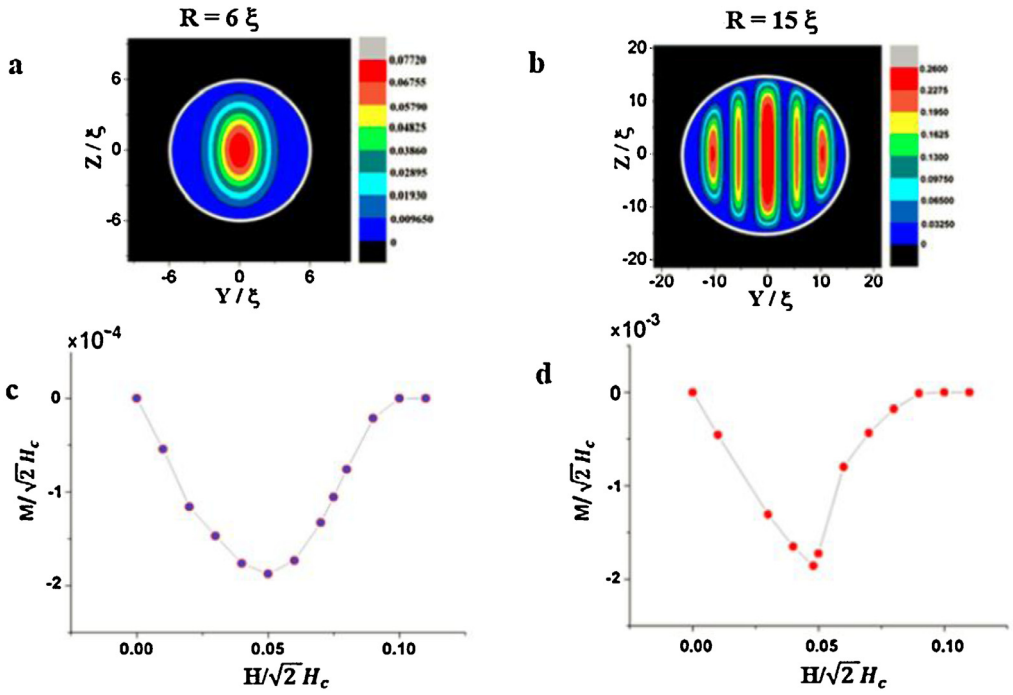

Fig. 6. Intermediate state for a type-I superconducting sphere in the YZ plane. (a) For a sphere with R = 6ξ, $\kappa = 0.22$, calculated at H = 0.09 and T = 0.5T_c. (b) For R = 15ξ, $\kappa = 0.18$, H = 0.07 and T = 0.5T_c. The white circles denote the border of the sphere in the YZ plane. Calculated magnetization curves for the spheres with R = 6ξ (c) and R = 15ξ (d).

using a rectangular Cartesian grid, embedding the sphere in a cube of size $L > R$. The magnetic field is applied in the z-direction, defining $H = H_z$ as the boundary conditions on the cube sides.

A link-variables approach method [28] was applied to solve numerically the set of Eq. (10) up to a stationary state for a given external magnetic field. The stationary state solution provides the local magnetic field inside the sphere $H(r)$ and the magnetic induction $B = \int H(r)d^3r / \int d^3r$. The magnetization $M(H)$, in units of $\sqrt{2}\ H_c$, is calculated from $M = (B - H)/4\pi$.

The numerical simulations provide the structure of the intermediate state for the spheres. Fig. 6a shows the calculated density of the superconducting phase $n_s = |\psi|^2$ in the YZ plane inside a sphere of R = 6ξ, $\kappa = 0.22$, for H = 0.09 and T = 0.5T_c. Apparently, only one superconducting domain, surrounded by a normal phase, is observed. The normal phase continuously invades the sphere as the field increases. Evidently, in our experiment the radius of both S and L spheres (~60 and ~700 nm, respectively) is less than 6ξ. Thus, one may expect that the intermediate state in both of these samples consists of only one superconducting domain.

A more complex intermediate state is obtained in the simulations for large spheres. This is demonstrated in Fig. 6b that shows the density of the superconducting phase inside a sphere of R = 15ξ, $\kappa = 0.18$, H = 0.07 and T = 0.5T_c. Several superconducting domains are now observed, separated by normal domains. Interestingly, images in the XY plane (not shown here) reveal that the intermediate state of the large sphere includes clusters of vortices surrounded by the superconducting phase [27]. A more detailed description of the intermediate state in type-I spheres and its dependence on size, temperature and field, will be published elsewhere [29].

The calculated $M(H)$ for the spheres of Fig. 6a and b are shown in Fig. 6c and d, respectively. A pronounced difference between the two magnetization curves is observed in the initial drop of M vs. H after the minimum in M. The sharp drop of M in the large sample is associated with an abrupt change in the topology of the superconducting phase, from a simply connected single domain at H = 0.05 to a multiply connected domain at H = 0.07. The absence of such a sharp drop in the experimental data for samples S and L is consistent with the above expectation that the intermediate state in these samples consists of only one simply connected superconducting domain surrounded by a normal region.

5. Summary and conclusions

Magnetic measurements in carbon-coated tin spheres with size smaller than the coherence length, ξ_0, of clean tin, show type-I superconductivity with a critical field, H_c, similar to that of bulk tin. The absence of the expected increase in H_c is attributed to carbon doping which significantly decreases the effective coherence length below the size of these spheres. Simulations based on the TDGL equations explains the measured gradual drop in the magnetization curves as resulting from an intermediate state consisting of only one superconducting domain surrounded by a normal domain. This normal domain invades the sphere gradually as the external field increases. The simulations also predict a rich multi-domain structure in larger Sn spheres, a prediction that has yet to be experimentally confirmed.

Acknowledgements

The experimental work was partially supported by the Israel Science Foundation (ISF) and the German-Israeli Foundation (GIF). The theoretical work and simulations were co-funded by the European Regional Development Fund and the Republic of Cyprus through the Research Promotion Foundation (Project Cy-Tera NEA ΥΠΟΔΟΜΗ/ΣΤΡΑΤΗ/0308/31).

References

[1] Y. Guo, Y.-F. Zhang, X.-Y. Bao, T.-Z. Han, Z. Tang, L.-X. Zhang, W.-G. Zhu, E. Wang, Q. Niu, Z. Qiu, Superconductivity modulated by quantum size effects, Science 306 (2004) 1915–1917.

[2] W.-H. Li, C.-W. Wang, C.-Y. Li, C. Hsu, C. Yang, C.-M. Wu, Coexistence of ferromagnetism and superconductivity in Sn nanoparticles, Phys. Rev. B 77 (2008) 094508.
[3] A. Müller, M.V. Milošević, S.E. Dale, M.A. Engbarth, S.J. Bending, Magnetization measurements and Ginzburg–Landau simulations of micron-size β-tin samples: evidence for an unusual critical behavior of mesoscopic type-I superconductors, Phys. Rev. Lett. 109 (2012) 197003.
[4] S. Bose, P. Ayyub, A review of finite size effects in quasi-zero dimensional superconductors, Rep. Progr. Phys. 77 (2014) 116503.
[5] M. Das, B. Wilson, Novel superconductivity: from bulk to nano systems, Adv. Nat. Sci. 6 (2014) 013001.
[6] I. Lukyanchuk, V. Vinokur, A. Rydh, R. Xie, M. Milošević, U. Welp, M. Zach, Z. Xiao, G. Crabtree, S. Bending, Rayleigh instability of confined vortex droplets in critical superconductors, Nat. Phys. 11 (2015) 21–25.
[7] I. Giaever, H. Zeller, Superconductivity of small tin particles measured by tunneling, Phys. Rev. Lett. 20 (1968) 1504.
[8] S. Reich, G. Leitus, R. Popovitz-Biro, M. Schechter, Magnetization of small lead particles, Phys. Rev. Lett. 91 (2003) 147001.
[9] J.E. Han, V.H. Crespi, Discrete transverse superconducting modes in nanocylinders, Phys. Rev. B 69 (2004) 214526.
[10] L. Jankovic, D. Gournis, P.N. Trikalitis, I. Arfaoui, T. Cren, P. Rudolf, M.-H. Sage, T.T. Palstra, B. Kooi, J. De Hosson, Carbon nanotubes encapsulating superconducting single-crystalline tin nanowires, Nano Lett. 6 (2006) 1131–1135.
[11] Y.J. Hsu, S.Y. Lu, Y.F. Lin, Nanostructures of Sn and their enhanced, shape-dependent superconducting properties, Small 2 (2006) 268–273.
[12] V. Yeh, S. Wu, W.-H. Li, Measurements of superconducting transition temperature T c of Sn nanoparticles, Colloids Surf. A 313 (2008) 246–249.
[13] X.-L. Wang, M. Feygenson, M.C. Aronson, W.-Q. Han, Sn/SnO x core− shell nanospheres: synthesis, anode performance in Li ion batteries, and superconductivity, J. Phys. Chem. C 114 (2010) 14697–14703.
[14] Y. Zhang, C.H. Wong, J. Shen, S.T. Sze, B. Zhang, H. Zhang, Y. Dong, H. Xu, Z. Yan, Y. Li, Dramatic enhancement of superconductivity in single-crystalline nanowire arrays of Sn, Sci. Rep. 6 (2016).
[15] V.B. Kumar, A. Gedanken, G. Kimmel, Z.E. Porat, Ultrasonic cavitation of molten gallium: formation of micro-and nano-spheres, Ultrasonics Sonochem. 21 (2014) 1166–1173.
[16] V.G. Pol, P. Thiyagarajan, S. Acharya, K. Ariga, I. Felner, Superconducting nanocrystalline tin protected by carbon, Langmuir 25 (2009) 2582–2584.
[17] M. Tinkham, Introduction to Superconductivity, 2nd ed., Books on Physics, Dover, 2004.
[18] E. Lynton, B. Serin, M. Zucker, The superconductive critical temperature and the electronic specific heat of impur1e tin, J. Phys. Chem. Solids 3 (1957) 165–174.
[19] J. Feder, D.S. McLachlan, Superheating and supercooling in single spheres of tin, indium, and gold-plated indium, Phys. Rev. 177 (1969) 763.
[20] R. Huebener, Magnetic Flux Structures in superconductors: Extended Reprint of a Classic Text, 2nd ed., Springer Science & Business Media, 2001.
[21] R. Prozorov, Equilibrium topology of the intermediate state in type-I superconductors of different shapes, Phys. Rev. Lett. 98 (2007) 257001.
[22] Superconductivity, Markel Dekker Inc, 1969.
[23] N.B. Kopnin, Theory of Nonequilibrium Superconductivity, Oxford University Press, 2001.
[24] V.L. Ginzburg, Nonequilibrium Superconductivity, Nova Publishers, 1988.
[25] I. Shapiro, E. Pechenik, B.Y. Shapiro, Recovery of superconductivity in a quenched mesoscopic domain, Phys. Rev. B 63 (2001) 184520.
[26] R.E. Goldstein, D.P. Jackson, A.T. Dorsey, Current-loop model for the intermediate state of type-I superconductors, Phys. Rev. Lett. 76 (1996) 3818.
[27] M.M. Doria, A.R.D.C. Romaguera, F. Peeters, Effect of the boundary condition on the vortex patterns in mesoscopic three-dimensional superconductors: disk and sphere, Phys. Rev. B 75 (2007) 064505.
[28] E. Coskun, M.K. Kwong, Simulating vortex motion in superconducting films with the time-dependent Ginzburg-Landau equations, Nonlinearity 10 (1997) 579.
[29] B. Shapiro, I. Shapiro, Unpublished.